

PSI Experiment R-05-01 (PEN)

Precise Measurement of the $\pi^+ \rightarrow e^+ \nu$ Branching Ratio

Progress Report and Beam Request

L. P. Alonzi^a, V. A. Baranov^c, W. Bertl^b, M. Bychkov^a, Yu.M. Bystritsky^c, E. Frlež^a,
V.A. Kalinnikov^c, N.V. Khomutov^c, A.S. Korenchenko^c, S.M. Korenchenko^c, M. Korolija^f,
T. Kozłowski^d, N.P. Kravchuk^c, N.A. Kuchinsky^c, D. Mekterović^f, D. Mzhavia^{c,e}, A. Palladino^{a,b},
D. Počanić^{a*}, P. Robmann^g, A.M. Rozhdestvensky^c, S.N Shkarovskiy^c, U. Straumann^g,
I. Supek^f, P. Truöl^g, Z. Tsamalaidze^e, A. van der Schaaf^{g*}, E.P. Velicheva^c, and V.P. Volnykh^c

^a*Department of Physics, University of Virginia, Charlottesville, VA 22904-4714, USA*

^b*Paul Scherrer Institut, CH-5232 Villigen PSI, Switzerland*

^c*Joint Institute for Nuclear Research, RU-141980 Dubna, Russia*

^d*Instytut Problemów Jądrowych im. Andrzeja Sołtana, PL-05-400 Świerk, Poland*

^e*IHEP, Tbilisi, State University, GUS-380086 Tbilisi, Georgia*

^f*Institut "Rudjer Bošković," HR-10000 Zagreb, Croatia*

^g*Physik Institut der Universität Zürich, CH-8057 Zürich, Switzerland*

(The PEN Collaboration)

19 January 2009

1. Summary of activities in 2008

The past year's PEN activities were carried out in accordance with the goals and priorities stated in our 2008 beam request, and in accordance with the overall goal to reach the uncertainty of $\delta B/B_{\text{tot}} \simeq 5 \times 10^{-4}$:

- to improve our data acquisition system so that it may handle a stop rate of $2 \times 10^4 \pi/\text{s}$, while maintaining an acceptable dead time fraction below 15%, and
- to record at least $4 \times 10^6 \pi \rightarrow e\nu$ events with well controlled systematics.

Both of these goals were met. During the 111 days scheduled for the run, the ring accelerator delivered 4.17 Ah of proton beam on the E production target, corresponding to 67% nominal availability. The experiment took pion beam for $6.51 \times 10^6 \text{ s}$ (75.4 days, or $\sim 90\%$ availability fraction), observing 7.46×10^{10} tagged pion stops in the target detector, and recording a total of some $4.6 \times 10^6 \pi \rightarrow e\nu$ decays before cuts.

*Co-spokesmen

Halfway during the 2008 measurements the one-piece active degrader introduced in 2007 and shown in Fig. 1, was replaced by a 4-piece wedged detector, WD. Its primary purpose is a rough determination of the trajectory of the incoming pion, needed for the measurement of the positron path length in the target, and thus for the predicted positron energy loss. Each wedge tapered from a thickness of 5 mm at the phototube end, to 1.5 mm at the far end, as seen in Fig. 2. The x, y coordinates of the pion trajectory can be determined with a precision of 1-2 mm by making use of the energy sharing over the four detector elements.

2. First results from the 2008 data analysis

The analysis of our 2008 data is still in its basic stage. We are presently pursuing the following objectives:

- optimizing the handling of each detector's data and its calibration,

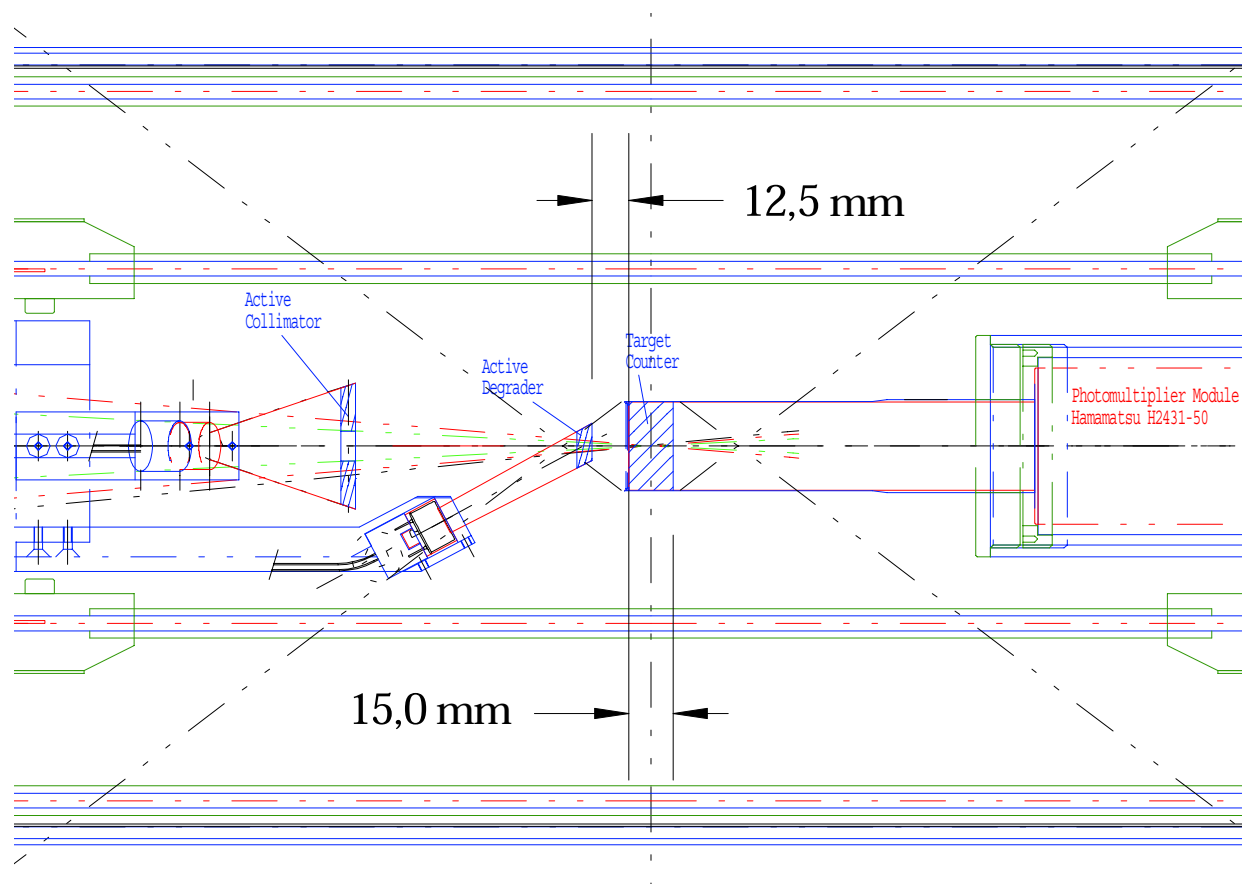


Figure 1:
Schematic drawing of the central-region beam detectors used in the 2007 and 2008 PEN runs: the active collimator, degrader, and active target. During the 2008 run the single thin degrader was replaced by the 4-piece wedged degrader, shown in Fig. 2.

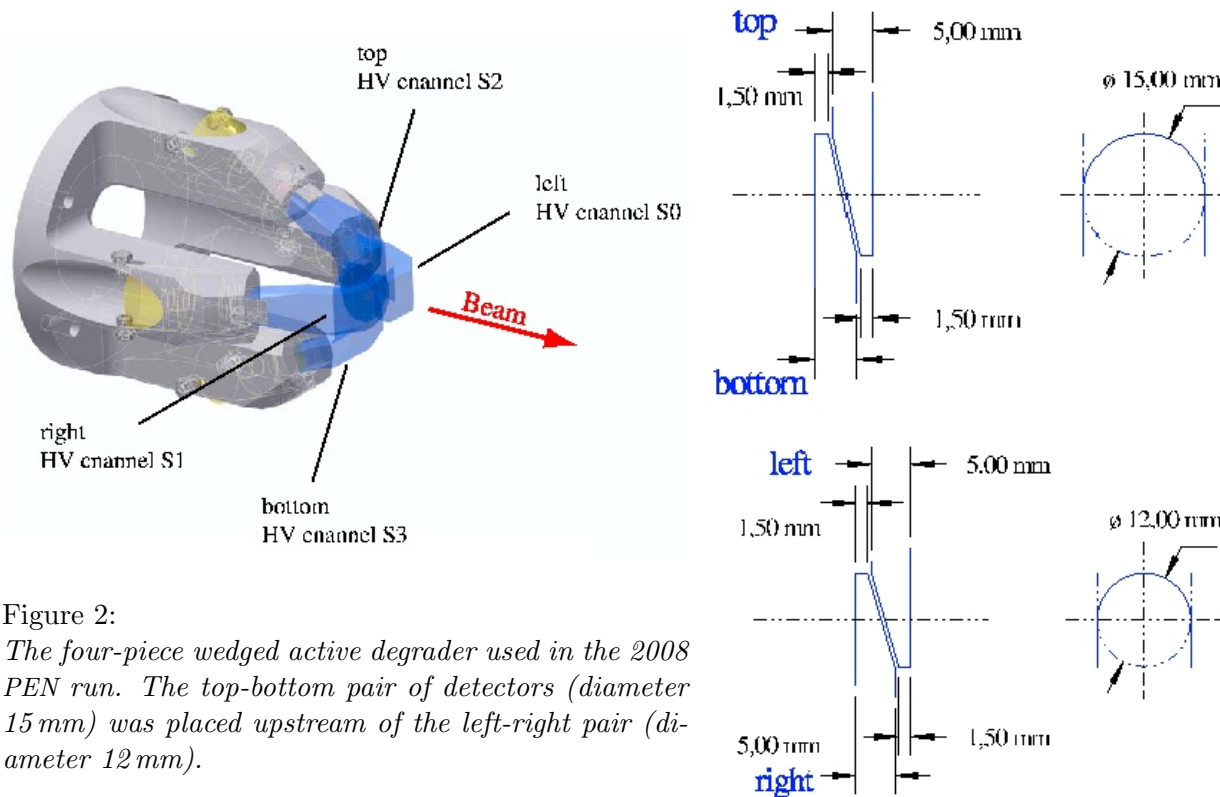


Figure 2:
The four-piece wedged active degrader used in the 2008 PEN run. The top-bottom pair of detectors (diameter 15 mm) was placed upstream of the left-right pair (diameter 12 mm).

- extracting the response functions for all detector components,
- optimizing the waveform fitting algorithms for efficiency and speed, and
- understanding in detail all sources of background.

Given the high aimed precision of the experiment, and the large volume of acquired data, we are taking great care in getting the basics right so that we do not need to revisit them.

2.1. Evaluation of the π_{e2} branching ratio

The primary method of evaluating the π_{e2} branching ratio, as outlined in the experiment proposal, is to normalize the observed yield of $\pi \rightarrow e\nu$ decays in a high-threshold calorimeter energy trigger (HT) to the number of sequential decays $\pi \rightarrow \mu \rightarrow e$ in an all-inclusive pre-scaled trigger (PT). To be accepted in either trigger, an event must contain the positron signal within a 250 ns gate which starts about 40 ns before the pion stop time. Although the branching ratio can be determined without observing the $\pi \rightarrow \mu\bar{\nu}$ decay, the efficient detection of the intermediate muon is of great help in reducing various sources of systematic error as will be discussed below.

2.2. Positron identification

Pion reactions in the target are an abundant source of protons with energies reaching far beyond the region of interest. Positrons are separated from other charged particles by their characteristic energy loss in the plastic hodoscope (see Fig. 3). Events above 2.5 MeV are removed from the sample which results in a very efficient suppression of prompt background.

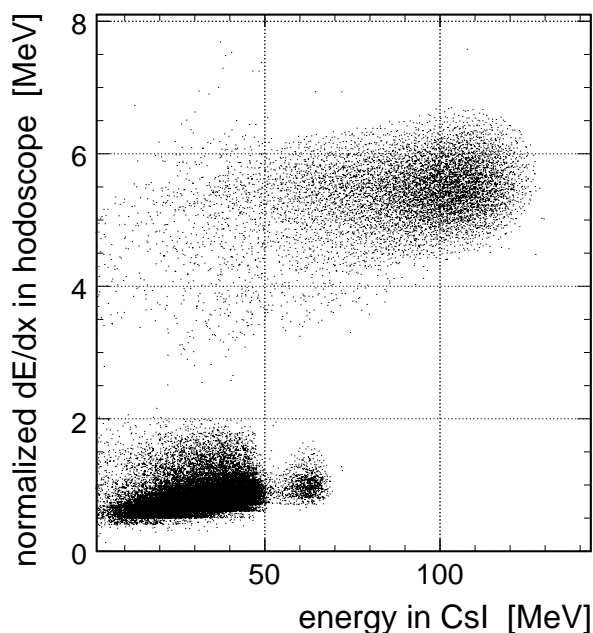


Figure 3:
Charged particle dE/dx corrected for the energy dependence observed for protons.

2.3. Analysis of the beam counter waveforms

The π_{e2} events within the HT data sample are identified by their energy and their time distribution with respect to the pion stop time reference. On the other hand, the pre-scaled trigger provides the corresponding number of sequential $\pi \rightarrow \mu \rightarrow e$ decays, again via their characteristic time and energy distributions. Additional information required for the branching ratio evaluation comes from the recorded target waveforms which allow us to separate π_{e2} events (two pulses in the target waveform: pion stop and decay positron), from the sequential decay events (three pulses in the target waveform, produced by the pion, muon and positron, respectively).

In a first step, the waveforms are filtered to remove tails and reflections caused by imperfect signal transmission to the 2 GS/s digitizers. The filtering is done in a single pass and does not depend on the individual waveforms. Figure 4 shows how the muon signal gets clipped to a symmetric shape with minimal loss in peak amplitude as well as minimal distortion of the baseline at distances larger than ± 4 ns. Pion and positron signals look very similar.

In the waveform fits signals are described numerically with 50 ps binning. Sample waveforms for both event types are illustrated in Fig. 5.

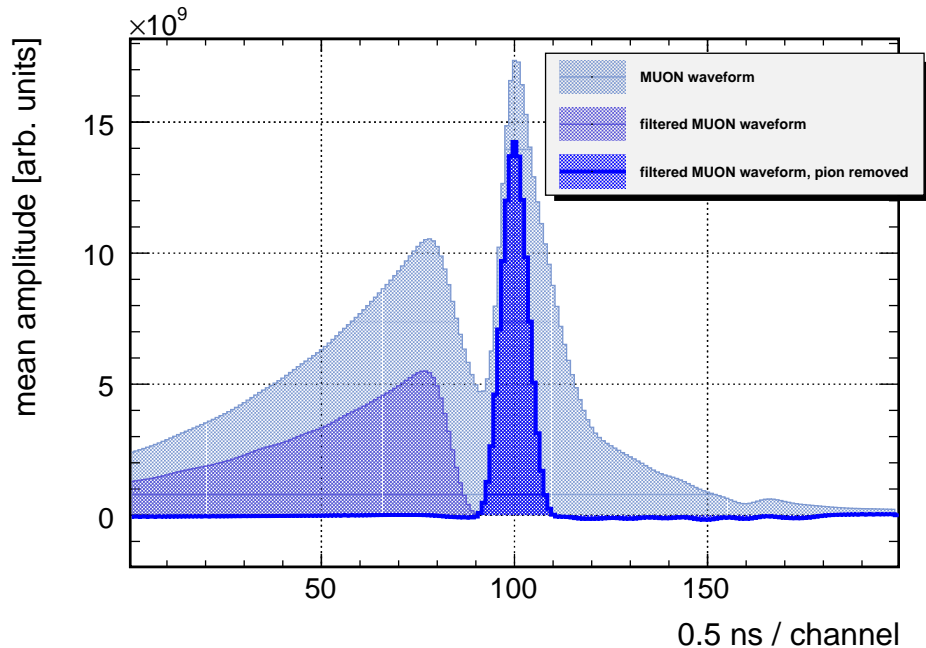


Figure 4:

Muon waveform in the target signal summed over many events. Baselines were corrected event by event, and the waveform polarity was flipped. Isolated muons were selected by requiring time delays of at least 10 ns with respect to the stopping pion, and at least 50 ns to the positron. Top to bottom: raw waveform, filtered waveform, and filtered waveform after subtraction of the pion signal.

The success of the waveform fitting of events with overlapping signals in the target depends critically on the allowed ranges for the positions (times) and amplitudes (energies) of the observed particles. The times of the pion and the positron are known to high precision from the degrader and the plastic hodoscope, respectively. Below, we present preliminary results obtained by analyzing the final two days of 2008 data taking. Figure 6 shows a scatter plot of the time delay between the degrader and target signals observed in the waveforms versus the observed pion energy. The observed 62 ps rms is an order of magnitude below the 500 ps binning of the waveforms.

Just as important as the times, energies deposited by the pion and the positron in the target can be predicted, as well.

The energy of the pion as it reaches the degrader is determined for each event from its time of flight. The energy of the pion as it enters the target is obtained in the next step, by subtracting the total energy observed in the degraders. Figure 7 shows a scatter plot of the observed and predicted values of the pion energy deposited in the target. A cross check can be made using the pion range which can be observed for $\pi \rightarrow e\nu$ events with positrons moving perpendicular to the beam direction, as shown in Fig.8. This plot demonstrates that the pion stop distribution is well contained in the 15 mm deep target, which is of critical importance, since our analysis assumes that all decay muons stay confined inside the target.

The positron energy in the target can be predicted from the reconstructed positron trajectory,

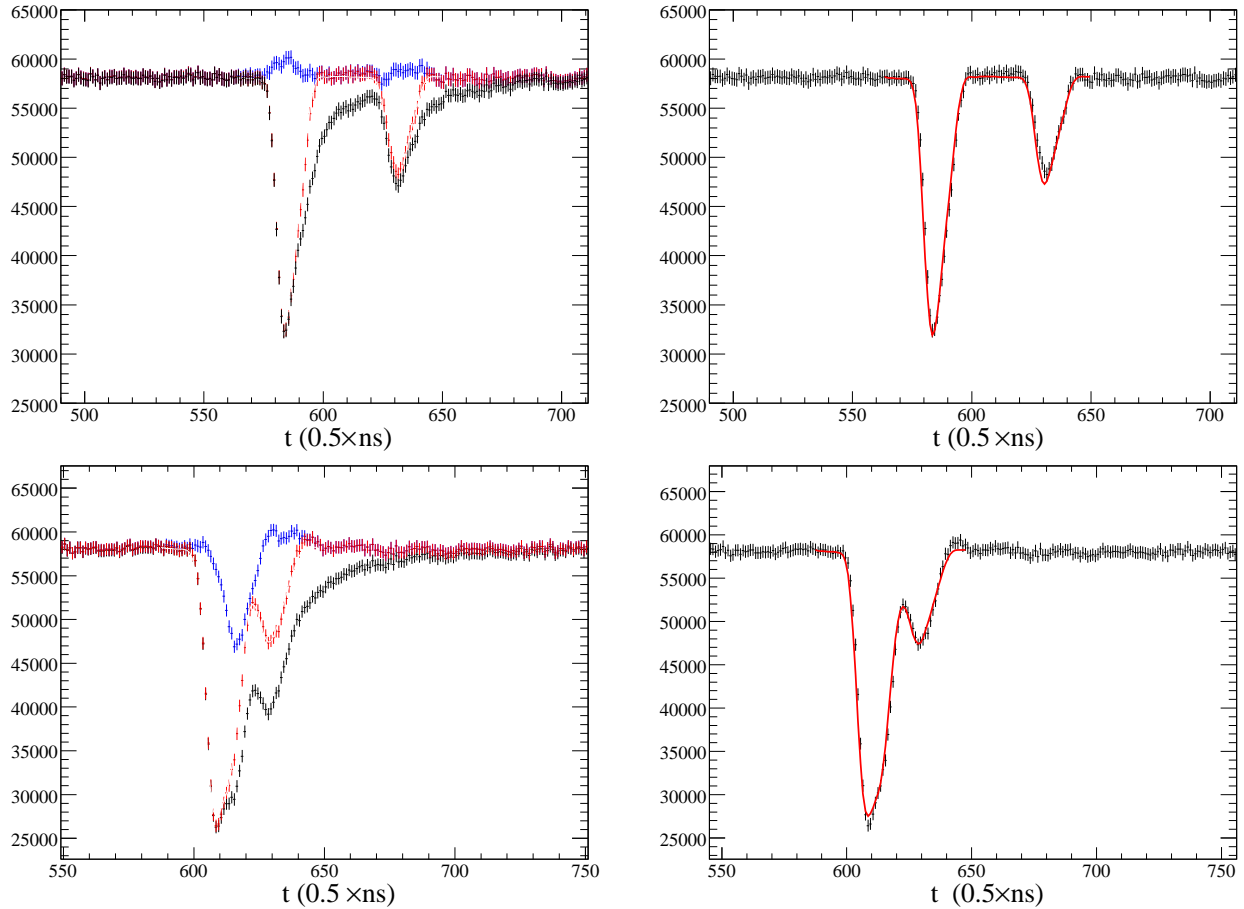


Figure 5:

Sample target waveforms for $\pi \rightarrow e \nu$ decay events (top), and $\pi \rightarrow \mu \rightarrow e$ sequential decay events (bottom). In the left panels black points depict the full original signal waveforms, while the red points depict the waveforms after digital filtering. The blue points show the waveform after the predicted pion and positron pulses are subtracted, as discussed in the text. For the $\pi \rightarrow e \nu$ event, the blue pulse shape is nil, while for the $\pi \rightarrow \mu \rightarrow e$ event, the leftover blue pulse belongs to the muon. Right panels show full filtered waveforms (black points) for the same two events, with superimposed fit (red curve) containing all two or three pulses, as appropriate. The $\pi \rightarrow \mu \rightarrow e$ sample waveform features relatively close π , μ , and e pulses, thus highlighting the challenge of reliable extraction of strongly overlapping signals.

although here the precision is hampered by the statistical fluctuations in the positron energy loss. In our geometry the spread in positron energy deposited in the target is quite large (see Fig. 10) and may approach the electron-equivalent energy deposited by the beam. As a result, precise modeling of the pion stop distribution is required for a proper description of the positron threshold region. The energy detected in the target is added to the energies observed in the plastic hodoscope and the CsI calorimeter.

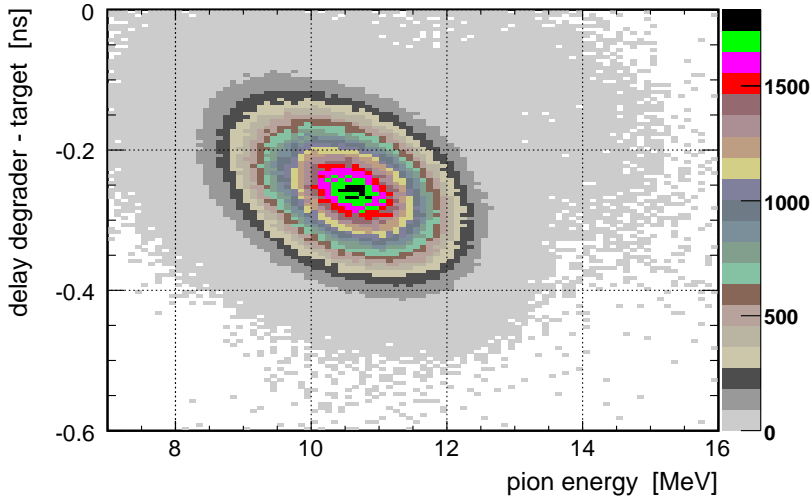


Figure 6:
Time delay between the weighted mean of the four degrader signals and the target signal versus pion energy. Correcting for the energy dependence a time resolution of 62 ps rms was obtained.

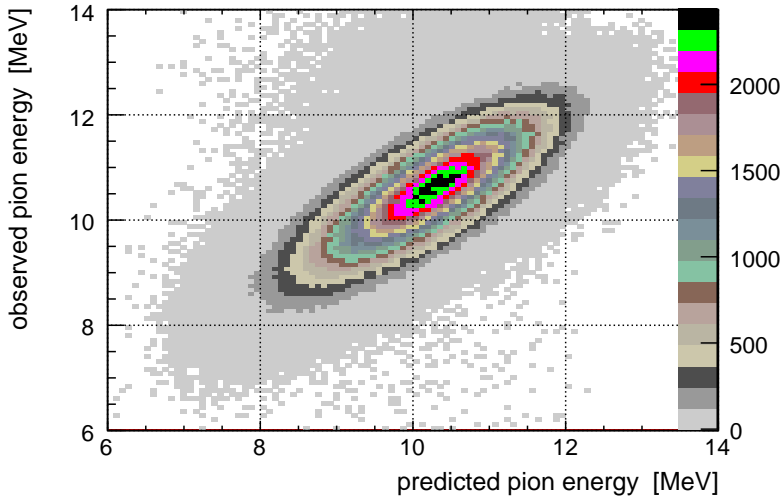


Figure 7:
Pion energy observed in the target, plotted against energy predicted from time of flight and energy loss observed in the degraders.

2.4. Separation of muon and positron final states

After removal of the pion and positron signals, a search is performed for an intermediate muon signal. Figure 9 shows a spectrum of the largest signal observed in the target waveform in the interval between pion stop and positron appearance. Besides π_{e2} decays, the pedestal peak receives contributions from pion decays in flight (resulting in a stopping muon), and from accidental coincidences for which the pion was still alive by the time of the positron appearance. The signals above the muon peak show a pronounced 50 MHz structure, and can thus be interpreted as accidental beam particles. The tail on the low-energy side is probably caused by the radiative decay $\pi \rightarrow \mu\nu\gamma$, which has a branching ratio of $O(10^{-4})$ for photon energies relevant for this plot.

Identified π_{e2} events serve to map out the energy response function of the setup, enabling us to evaluate the low energy “tail” in the region dominated by muon decays. A preliminary result of a calorimeter low-energy tail analysis is presented in Fig. 11.

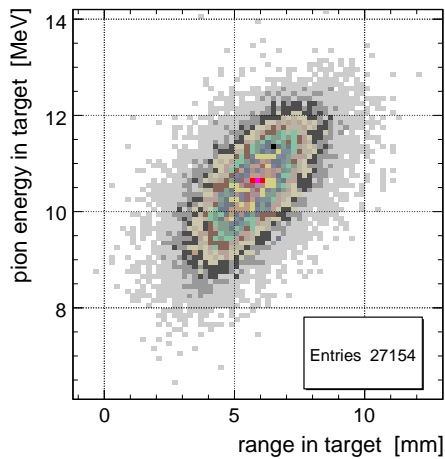


Figure 8:
Target energy versus range observed for $\pi \rightarrow e\nu$ decays with positron direction perpendicular (within 10°) to the beam axis.

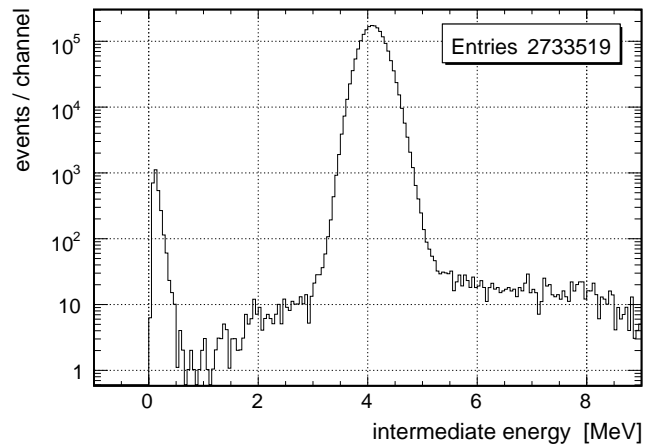


Figure 9:
Energy distribution of the largest signal observed in the target waveform between pion stop and positron appearance. Most prominent, with a yield of 99.9%, is the 4.1 MeV muon signal. The remaining components are discussed in the text.

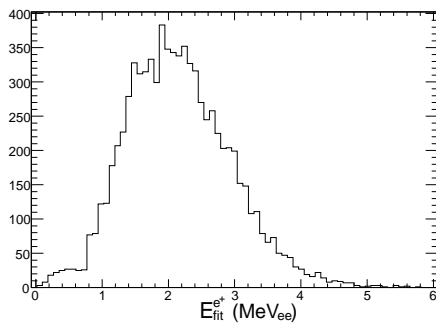


Figure 10:
Spectrum of fitted positron energy in the target detector. There is virtually no difference in the target positron energy spectra for $\pi \rightarrow \mu \rightarrow e$ and $\pi \rightarrow e\nu$ decay events.

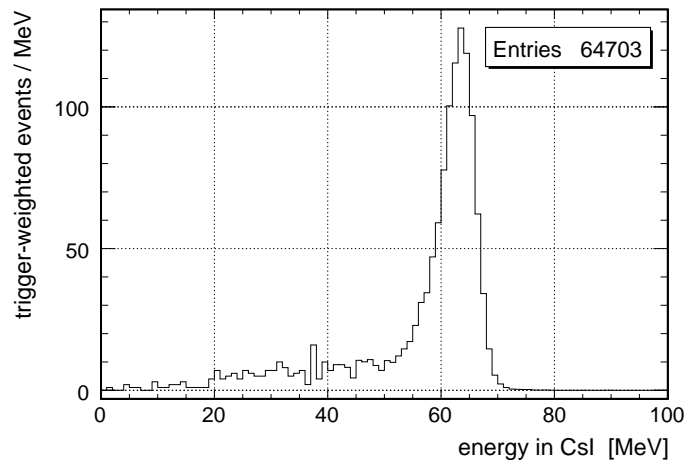


Figure 11:
Preliminary positron energy distribution for $\pi \rightarrow e\nu$ decays. The region below 50 MeV has about 50% background from accidental coincidences and pion decay in flight. We intend to reduce these backgrounds as the data analysis is refined. This particular data set was taken at a relatively high pion stop rate of $2 \times 10^4 \text{ s}^{-1}$.

Reliable observation of the intermediate muon allows for an alternative method for the determination of the π_{e2} branching ratio. Figure 12 illustrates how well the two event types can be separated on the basis of the recorded waveforms, indicating that it may be feasible to deduce the

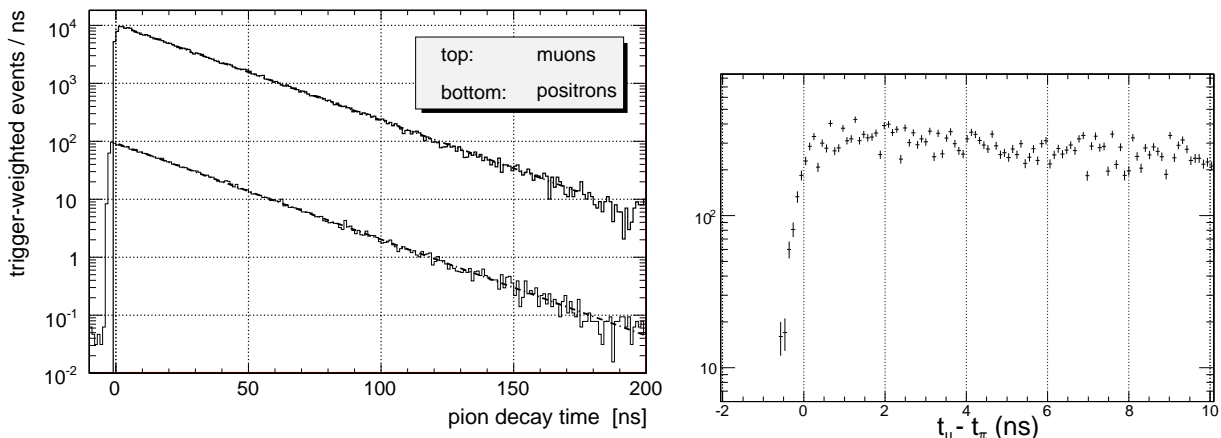


Figure 12:

Left: distributions of pion decay time for muon and positron final states. For $\pi \rightarrow \mu\nu$ events a subsequent $\mu \rightarrow e\nu\bar{\nu}$ decay was required in a time window 5 – 25 ns after the pion decay. The observed life times, ignoring accidental background, are 26.21(5) ns for the muon and 26.02(8) ns for the positron final state. The statistical accuracy of the two samples is similar given the prescaling factor 1:64 between the pre-scaled (PT) and high-threshold (HT) triggers.

Right: spectrum of pion–muon pulse time differences obtained in fits of $\pi \rightarrow \mu \rightarrow e$ event target waveforms, as illustrated in Fig. 5, demonstrating the ability to separate the two processes down to time zero.

branching ratio by summing the two event types, and correcting for the fraction of muons decaying in the chosen $\mu \rightarrow e$ time window. The precise location of this window is not very critical on the time scale of the muon lifetime. The method would require reliable and efficient identification of the presence or absence of the muon pulse in the target waveform, as illustrated in Fig. 5. The present state of the art is reflected in the decay time histogram for $\pi \rightarrow \mu$ events resulting from the waveform fit, shown in the right panel of Fig. 12. There is no observable diminution of efficiency as $\Delta t_{\mu-\pi} \rightarrow 0$. The slight roll-off at $\Delta t = 0$, and the associated spillover into the unphysical interval $-250 \text{ ps} \leq \Delta t_{\mu-\pi} \leq 0$ is induced by waveform sampling noise which can favor placing the muon pulse marginally before the pion pulse in an unconstrained fit.

3. Simulations

Ideally, the determination of the branching ratio should be done independent of event simulation, as the latter could be a source of systematic errors in itself. Nevertheless, we intend to reproduce our observations to a level significantly below the requirements dictated by the branching-ratio sensitivity we plan to achieve.

Simulations are needed to account for potential differences between the two processes related to the positron energy (threshold effects, multiple scattering), the finite muon range, and radiative corrections. Simulations are also required to estimate the impact of various background processes such as decays in flight. Two distinct classes of pion decay in flight exist, i.e., decays occurring (a) in front, and (b) inside the target detector. The former can be identified and controlled for by

implementing a position sensitive detector between a thin degrader and the target, with accurate directional information in addition to the position measurement. A very suitable device for this purpose is a time projection chamber (TPC). We have designed for 2009 just such a mini-TPC, discussed below.

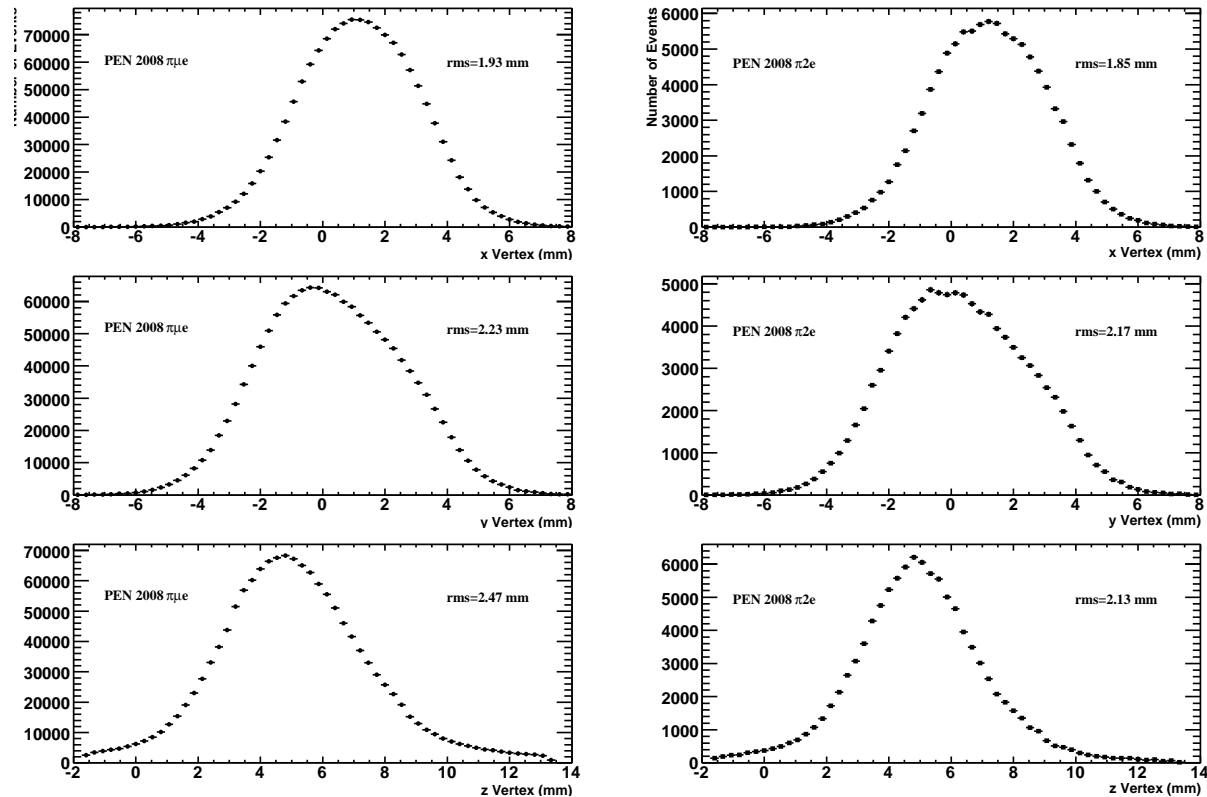


Figure 13:

Vertex coordinates of the points of closest approach between positron and pion trajectories for $\pi \rightarrow \mu \rightarrow e$ (left panel) and $\pi \rightarrow e \nu$ events (right panel). The trajectories are reconstructed using the WD and MWPC information.

To illustrate the performance of the wedged degrader, in Fig. 13 we present the fit results for both $\pi \rightarrow \mu \rightarrow e$ and $\pi \rightarrow e \nu$ decays for the point of closest approach to the positron and pion trajectories, reconstructed from the available MWPC and WD information for the positron and pion, respectively. The distributions are matched closely for the two classes of events, with the $\pi \rightarrow e \nu$ z distribution being slightly narrower than that of the $\pi \rightarrow \mu \rightarrow e$ events. Our GEANT simulations indicate that the WD yields ~ 2 mm position resolution, compared to ± 8 mm without. On the other hand, the PEN target systematic uncertainty would benefit from higher, sub-millimeter resolution. The position resolution is limited primarily by multiple scattering of pions in the WD material. Hence, a low-mass tracking detector, such as a time projection chamber discussed in the original PEN experiment proposal, would be required. The mini-TPC solution has the additional advantages of providing excellent directional information for the trajectories, thus enhancing our ability to identify pion decays in flight. Just as importantly, the mini-TPC low mass will significantly reduce the pion energy loss prior to the target, allowing us to lower the beam momentum, and thus the uncertainty in the prediction of the energy of the pion as it enters the target.

4. Modifications for 2009

4.1. The mini-TPC

As indicated above, we have undertaken to construct and implement a mini-TPC detector to replace the WD used in the 2008 run. The mini-TPC will be placed between a thin plastic scintillator degrader detector (DEG) and the active target. The mini-TPC physical design is shown in a schematic drawing in Fig. 14. Equipotential contours and electron drift lines calculated with the GARFIELD program, are shown in Fig. 15.

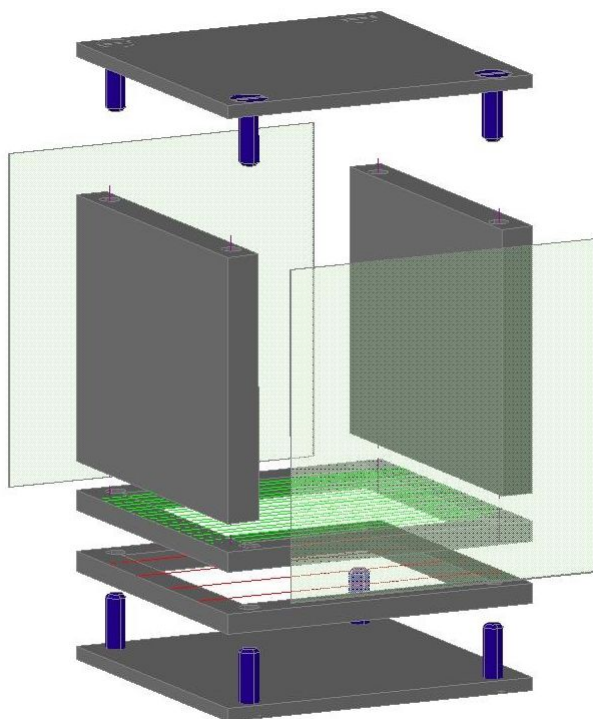


Figure 14:
A schematic drawing of the PEN mini-TPC beam tracker's physical design.

The detector is presently under construction in Dubna, and will be ready for deployment in February 2009.

4.2. Electronics upgrade

Another identified deficiency in our data set concerns the timing resolution of the thin hodoscope detector (formerly labeled “plastic veto”) array. At present, this is limited by the 0.5 ns least significant bit (LSB) readout resolution of the LeCroy FastBus TDCs currently in use. To remove this bottleneck we have placed an order for CAEN V1190A VME multihit TDCs, as well as V1720 waveform digitizers for the mini-TPC readout. The additional VME crate will be incorporated into the DAQ scheme along with a new hardware-based system for providing proper synchronization of the frontends.

In view of the difficulties experienced with the LB-102 fast logic units in the 2008 run, we are actively considering replacing them with more reliable units.

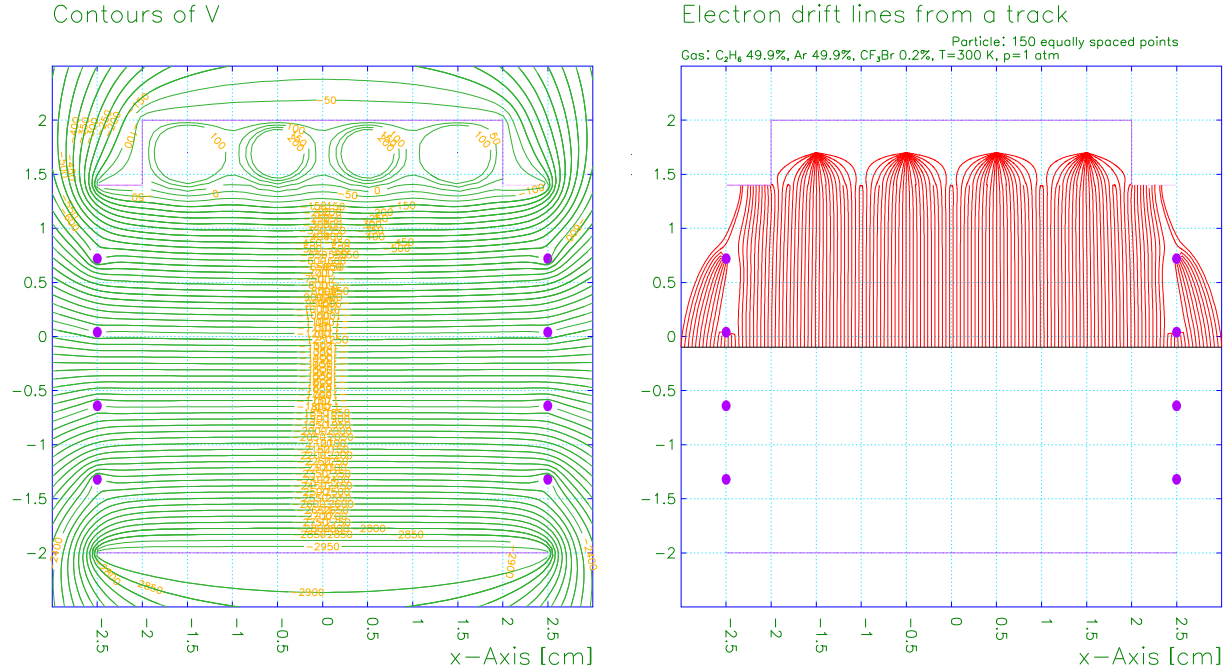


Figure 15:

Left: GARFIELD simulations of the equipotential contours in the drift volume of the planned PEN mini-TPC tracker, at $HV_{\text{drift}} = 3000 \text{ V}$ (left panel).

Right: the corresponding electron drift lines, also simulated using GARFIELD. Drift velocity varies less than 0.02% in the entire drift region.

5. Resources and beam request

We request 19 weeks of beam time in the πE1 beam area, which includes four weeks for setup and calibration, and 15 weeks of data taking. The requested setup and calibration time is somewhat longer to accommodate the move-in of the detector into the area.

Under our planned running condition, this amount of beam time would let us acquire more than 5×10^6 π_{e2} decay events, which, combined with earlier data, would allow us to approach our target statistical uncertainty of $\delta B/B \simeq 2 - 3 \times 10^{-4}$. In view of the planned detector upgrades and the Laboratory's use plan for the area, we request that our beam time be allocated in the second half of the Ring Accelerator 2009 beam delivery period.

There are no major costs associated with the requested run. The main expenditures are the material costs of operating the detector (MWPC gas, supplies, consumables), and modest amounts to support certain local expenses at PSI for collaborators from former socialist countries, similar to the 2008 budget.